DOI: 10.1002/chem.200501459

Ethylene Biosynthesis by 1-Aminocyclopropane-1-Carboxylic Acid Oxidase: A DFT Study

Arianna Bassan,*[a] Tomasz Borowski,*[b] Christopher J. Schofield,[c] and Per E. M. Siegbahn*[d]

Abstract: The reaction catalyzed by the plant enzyme 1-aminocyclopropane-1-carboxylic acid oxidase (ACCO) was investigated by using hybrid density functional theory. ACCO belongs to the non-heme iron(II) enzyme superfamily and carries out the bicarbonate-dependent two-electron oxidation of its substrate ACC (1-aminocyclopropane-1-carboxylic acid) concomitant with the reduction of dioxygen and oxidation of a reducing agent probably ascorbate. The reaction gives ethylene, CO_2, cyanide and two water molecules. A model including the mononuclear iron complex with ACC in the first coordination sphere was used to study the details of O–O bond cleavage and cyclopropane ring opening. Calculations imply that this unusual and complex reaction is triggered by a hydrogen atom abstraction step generating a radical on the amino nitrogen of ACC. Subsequently, cyclopropane ring opening followed by O–O bond heterolysis leads to a very reactive iron(IV)–oxo intermediate, which decomposes to ethylene and cyanoformate with very low energy barriers. The reaction is assisted by bicarbonate located in the second coordination sphere of the metal.

Keywords: density functional calculations · ethylene · nonheme iron enzymes · reaction mechanisms

Introduction

The signaling molecule ethylene plays a crucial role in many aspects of plant physiology and development,[1–3] including for example fruit ripening, seed germination, flower senescence, responses to hypoxia, and leaf abscission. In higher plants, the biosynthesis of the smallest olefin starts with the conversion of S-adenosyl-L-methionine (SAM) to 1-aminocyclopropane-1-carboxylic acid (ACC) by ACC synthase.[4] The ethylene-forming enzyme, ACC oxidase (ACCO), then catalyzes the conversion of ACC to ethylene (see Figure 1).

ACCO (its crystal structure has been recently solved)[5] belongs to the mechanistic superfamily of mononuclear nonheme iron(II) enzymes[6,7] that includes extradiol cleaving catechol dioxygenases, Rieske dioxygenases, α-ketoglutarate-dependent enzymes, pterin-dependent hydroxylases, isopenicillin N synthase and fosfomycin epoxidase.[8] Al-

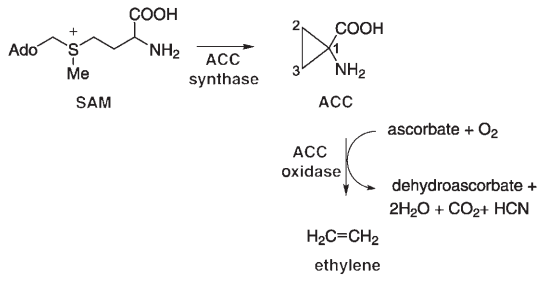

Figure 1. Ethylene biosynthesis by ACC synthase and ACC oxidase (ACCO).

[a] Dr. A. Bassan
Department of Physics, Stockholm Center for Physics Astronomy and Biotechnology, Stockholm University
10691 Stockholm (Sweden)
Fax: (+46) 855-378-601
E-mail: arianna@physto.se

[b] Dr. T. Borowski
Institute of Catalysis and Surface Chemistry
Polish Academy of Sciences, ul. Niezapominajek 8
30-239 Cracow (Poland)
E-mail: ncborows@cyf-kr.edu.pl

[c] Prof. C. J. Schofield
Oxford Centre for Molecular Sciences and Department of Chemistry
University of Oxford, Oxford OX1 3TA (UK)

[d] Prof. P. E. M. Siegbahn
Department of Physics, Stockholm Center for Physics Astronomy and Biotechnology, Stockholm University
10691 Stockholm (Sweden)
Fax: (+46) 855-378-601
E-mail: ps@physto.se

Supporting information for this article is available on the WWW under http://www.chemeurj.org/ or from the author.

though the overall folding patterns of these enzymes can differ, they use a common metal binding structural motif, the so called "2-His-1-carboxylate" facial triad,[8–10] to anchor a ferrous ion in the active site. Two histidines and a carboxylate group provided by endogenous glutamate or aspartate occupy three vertices of the iron octahedral coordination, which, in the resting state of these enzymes, is usually completed by water molecules. Most commonly, and as found in ACCO, the iron-binding residues are supported in conserved positions in a double stranded β-helix fold. This type of environment creates a weak ligand field and stabilizes the high-spin state of the metal.[7] The iron center is utilized by the enzymes to activate dioxygen[11] and to couple the four-electron reduction of O_2 with a wide spectrum of oxidation reactions, such as mono- and dihydroxylations, desaturation, heterocyclic ring formation, and C–C-bond cleavage.

In ACCO reduction of dioxygen to two water molecules is coupled with the decarboxylation of ACC and, probably, two-electron oxidation of ascorbate, producing dehydroascorbate (either directly or indirectly via semi-dehydroascorbate radicals) together with ethylene, HCN, and CO_2 (see Figure 1). C2 and C3 of ACC provide the carbon atoms of ethylene, while C1 and the amino group are incorporated into HCN, and the ACC carboxyl group instead generates CO_2.[2,12] The reaction catalyzed by ACCO is rather complex in that the enzyme requires not only ascorbate as cofactor but also CO_2 or bicarbonate as activator, which notably is also a product of the reaction.[13–16] So far, it is not fully clear if the actual activator is CO_2 or HCO_3^-; inhibition of ACCO activity by borate, an anion analogous to bicarbonate, was interpreted as an indication that HCO_3^- (or CO_3^{2-}) and not CO_2 plays the role of activator.[16]

The chemical transformations occurring in the ACCO active site are likely to involve a substrate radical as demonstrated by previous studies,[17] but the exact mechanism generating it is unknown. The use of NO as surrogate for O_2 gave crucial insights into the mechanism.[18,19] The ACCO nitrosyl adducts, which could be investigated by means of EPR and ENDOR spectroscopy, revealed that NO and two atoms of the ACC substrate bind simultaneously to iron. Furthermore, it was shown that the amino and the carboxyl groups of the inhibitor D,L-alanine, and thus in analogy with ACC, were engaged in the binding to iron. The conclusions drawn from these studies exclude a mechanism where dioxygen is activated through the direct binding of ascorbate to iron as previously proposed,[20] and they instead favor a catalytic cycle that involves the formation of an Fe^{II}-O_2-ACC complex. This scenario is supported by kinetic studies, which showed that ethylene could be produced in single turnover in the absence of ascorbate and in the presence of the CO_2 activator.[16] While in the single turnover experiments using isolated enzyme, the reduction equivalents needed for the reaction to occur could be provided by the free Fe^{II} in solution or possibly by the ferrous center of other ACCO monomers, in the steady state reaction ascorbate should play the role of best reductant. Besides its reducing activity, ascorbate was also found to act as an effector by increasing the rate of the reaction;[16] however, in the absence of ACC, ascorbate can enable oxidative damage to ACCO.[21]

The EPR and ENDOR studies led to the proposal of a reaction mechanism depicted in Figure 2.[16,18,19] In the resting

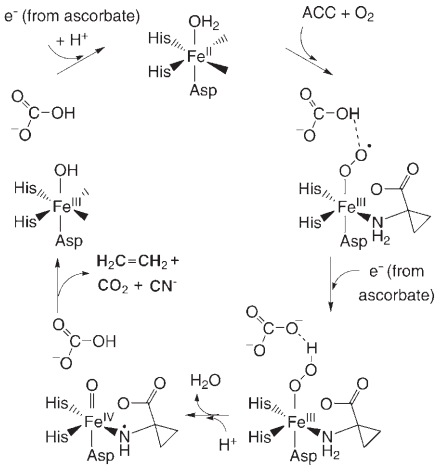

Figure 2. Proposed mechanism in the ethylene forming enzyme (ACCO).

state of the enzyme, iron is six-coordinate, hosting three endogenous ligands (two histidines and one aspartate) and three water molecules, which are substituted with ACC (bidentate binding) and O_2 (monodentate binding) upon activation with CO_2 and ascorbate. Because all the coordination sites are occupied at this stage of the reaction, it is unlikely that the activator bicarbonate (or CO_2) enters the first coordination sphere of the metal. It is instead proposed that bicarbonate binds in the vicinity of the iron complex, possibly to one of the (co)substrates. Ascorbate also facilitates the reaction by binding to the enzyme. It was previously proposed that at this initial stage of the reaction the two activators (bicarbonate and ascorbate) trigger the conversion of the iron complex from six- to five-coordinate in the presence of ACC,[22] thus leaving an open position available for dioxygen binding. The reaction proceeds with the reduction of the metal complex by ascorbate (or other reducing agents, possibly ACCO monomer in the case of single turnover experiments), generating an iron(II)–superoxo species, that upon protonation by bicarbonate becomes an Fe^{III}–hydroperoxide. O–O Bond cleavage assisted by bicarbonate together with deprotonation of ACC leads to a high-valent iron-oxo species, namely Fe^{IV}=O, and a substrate radical. This intermediate then fragments to produce ethylene, CO_2, HCN and an Fe^{III} complex. In the catalytic cycle, the initial ferrous state of the metal center is restored by a second electron provided by the ascorbate (or more precisely by a semidehydroascorbate radical). The ferric species is instead the product of the single turnover experiments, where ascorbate, and thus some of the reducing equivalents are missing.

In the current study, density functional theory with the hybrid functional B3LYP is employed to investigate the feasibility of the reaction mechanism depicted in Figure 2. The

computed energy barriers are used as guidelines to dismiss or accept mechanisms. The calculations are performed without including ascorbate in the model because conclusive experimental data regarding its binding and in vivo role are missing. Nevertheless, since single turnover studies indicated that ethylene production occurs also in its absence,[16] this investigation shed light on the possible mechanism of ethylene formation in ACCO, and more specifically on the role of bicarbonate, on the formation of an iron(IV)–oxo intermediate and on the degradation pathway of the substrate radical.

Computational Details

In the present investigation, reaction pathways were investigated by means of hybrid density functional theory with the B3LYP functional.[23–25] All the systems were characterized by open-shell electronic configurations and thus unrestricted DFT was used. The energy profiles presented in this work were obtained by means of the two quantum chemical programs Jaguar 4.2[26] and Gaussian 98.[27]

Transition states were located with the following procedure: initially a constrained optimization gave a guess structure whose Hessian (i.e., second derivatives with respect to the nuclear coordinates) was used to fully optimize the transition-state structure. Hessians were computed for all the stationary points (reactants, transition states and intermediates) in order to determine zero-point effects. Evaluation of the Hessian for optimized transition states was necessary to confirm that the structure is characterized by only one imaginary frequency corresponding to the normal mode associated with the reaction coordinate.

In the geometry optimizations and in the Hessian evaluations all the atoms but iron were described by a standard double ζ basis set, while an effective core potential and a double ζ basis set was used for the metal;[28,26] this basis set is labeled lacvp in Jaguar. The final B3LYP energies for the fully optimized structures were computed using a large basis set with polarization functions on all atoms, labeled lacv3p** in Jaguar.[26]

In order to reproduce the polarization effects of the enzyme environment, the self-consistent reaction field as implemented in Jaguar was employed.[29,30] The solvent was modeled as a homogeneous macroscopic continuum with dielectric constant $[\varepsilon] = 4.0$ and the solute as placed in a cavity contained in this continuous medium. The probe radius used to build the cavity was 2.5 Å. Final energies of the optimized structures were corrected for solvent effects by employing the B3LYP functional and the lacvp basis set.

In summary, relative energies and barriers presented in this work (referred as ΔE) are computed at the B3LYP/LACV3P**//B3LYP/LACVP level of theory and include zero-point and solvent effects evaluated with the lacvp basis set. Gibbs free energies are not generally provided because some coordinates of the models were fixed during geometry optimizations in order to mimic the rigidity provided by the protein platform. This approach would lead to large errors in the entropy evaluation by means of second derivatives. In a few cases, smaller models without any frozen coordinates have been used to evaluate the entropy correction ($-T\Delta S$).

Relevant spin populations as derived from the Mulliken population analysis and obtained with the lacvp basis set are reported. From these one can easily deduce where the unpaired electrons are located and which is the oxidation state of a metal. It has to be noted that for high-spin iron complexes the metal spin population does not strictly correspond to the number of d electrons expected for a given formal oxidation state. With the coordination environment dominated by oxygen- and nitrogen-donating ligands, the computed spin population on high-spin Fe^{II} ($S = 2$) is usually 3.7–3.8 and about 4.0–4.1 for high-spin Fe^{III} ($S = 5/2$).[31]

The accuracy of the B3LYP functional can be assessed from benchmark tests performed on a wide array of molecules (radicals, non-hydrogen systems, hydrocarbons, substituted hydrocarbons and inorganic hydrides)[32,33] and transition metal systems.[34–36] From the available data, it can be predicted that an error of about 3–5 kcal mol^{-1} would apply to the energy profiles reported in the present investigation. Such accuracy should be enough to discriminate among different reaction mechanisms.[37]

Results and Discussion

Model complex: The mechanism of ethylene biosynthesis has been investigated employing a model of the active site derived from the crystal structure of ACCO from *Petunia hybrida*,[5] where iron is coordinated by the side chains of His177, Asp179 and His234 (Figure 3). Following the proposed mechanism illustrated in Figure 2, ACC is considered to bind directly to the metal with the amino group bound trans to His177 and the carboxylate group bound trans to His234 as shown in the complex of Figure 4. A nearby asparagine (Asn216), which is likely to be engaged in a hydrogen bond interaction with the aspartate ligand, was also included in the model. Different binding modes of ACC are possible, which, however, could not be discriminated by means of the computational approach adopted in the current study. A model with the carboxylate group of ACC bound trans to Asp179 and the amino group bound trans to His234 was also tested, but since it provided similar results as the one in

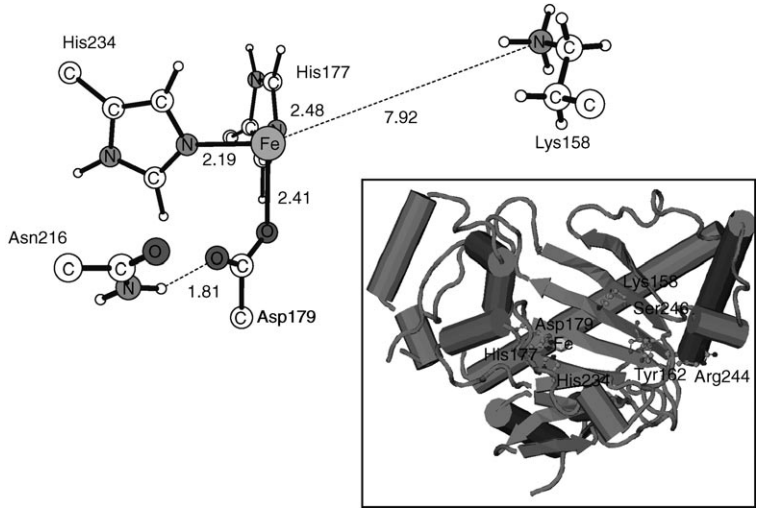

Figure 3. View from the active site of ACCO as observed in the crystal structure of the *Petunia hybrida* enzyme showing the iron binding and selected other residues. In the inset structure, some residues in the vicinity of the active site are shown.

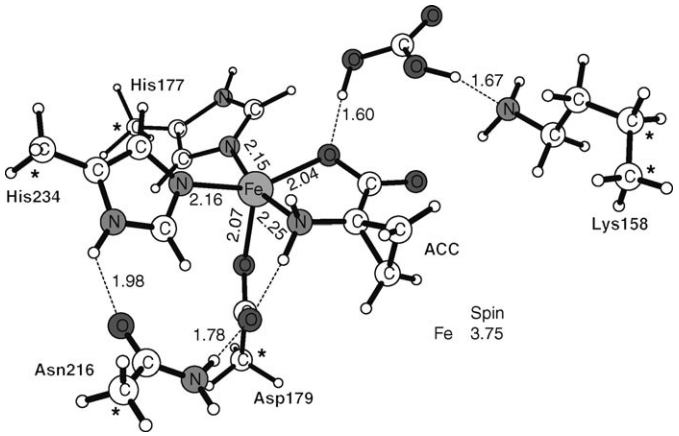

Figure 4. Iron(II) model complex including ACC and bicarbonate. Distances [Å] and spin populations from the S=2 optimized structure are shown. Atoms marked with an asterisk were kept frozen in the geometry optimizations of the present work.

Figure 4, it will not be discussed further although this mode of binding is possible during catalysis.

The possible role of bicarbonate as activator was investigated by placing the bicarbonate anion in the second coordination sphere of the metal. The side chain of the protonated form of Lys158, which extends into the active site, was chosen to anchor HCO_3^- as shown in Figure 4. There is no direct experimental evidence regarding the exact binding of bicarbonate in ACCO, and the choice to make it interact with the amino group of Lys158 is in part driven by the observation that in the crystal structure Lys158 is the positive residue closest to the metal center. Interestingly, site-directed mutagenesis experiments on ACCO from kiwi fruit shows a great loss of activity when Lys158 is substituted with Ala or Cys (the activity is reduced to less than 1% of the wild type activity).[38]

The model of the ACCO active site includes a bicarbonate anion binding to a protonated lysine cation. Geometry optimizations in gas phase tend to destroy the charge separation and lead to carbonic acid and unprotonated lysine (see Figure 4). It was found that this arrangement does not affect the investigated energetics and therefore the optimized structures presented below sometimes contain carbonic acid and neutral lysine instead of bicarbonate and protonated lysine.

To test the catalytic role of bicarbonate, separate calculations were performed for a model lacking the HCO_3^- group, but otherwise identical to the model described above. Such a model was employed to study only the rate-limiting steps of the catalytic reaction, which involve C–C and O–O bonds cleavage and lead from Fe^{II}-$O_2^{-\bullet}$ to Fe^{IV}=O species (see below).

In order to mimic the strain imposed by the protein fold, some atoms were kept frozen according to the available X-ray data as illustrated in Figure 4. The total charge of the complex is zero and the total spin of the ground state corresponds to a quintet. The free energy splitting between the low-spin and the high-spin states of the five-coordinate ferrous complex (S = 2 and S = 0) was calculated with a smaller model that did not include bicarbonate and protonated lysine. The low-spin coupling of the metal d electrons (singlet) was found to lie much higher in energy in agreement with experimental data indicating that this type of coordination environment (2-His-1-carboxylate motif) stabilizes the high-spin state of the ferrous ion.[7]

The iron(II)–dioxygen moiety: The five-coordinate iron complex (two imidazole ligands, a carboxylate and the bidentate ACC) has an open position for dioxygen binding, and more specifically O_2 can be accommodated trans to Asp179 (Figure 5). The computational method adopted in the present work gives energetic parameters for dioxygen binding in ACCO that does not differ much from those computed for enzymes belonging to the same mononuclear non-heme iron(II) superfamily,[31] such as aromatic amino acid hydroxylases,[39] α-ketoglutarate-dependent oxygenases[40] and naphthalene dioxygenase.[41] In those studies it was found that binding of molecular oxygen to the enzyme–Fe^{II} complex occurs with iron in the high spin state and the process was found to be endergonic due to a high entropic contribution ($-T\Delta S$ is on the order of 10 kcal mol^{-1} for this bimolecular reaction), which is not balanced by the enthalpic binding energy of approximately zero kcal mol^{-1}.[31,41]

Relative energies and corresponding spin populations of different spin states of the ACC-Fe^{II}-O_2 complex (S = 1,2, and 3) are reported in Table 1. The triplet state (S = 1) is

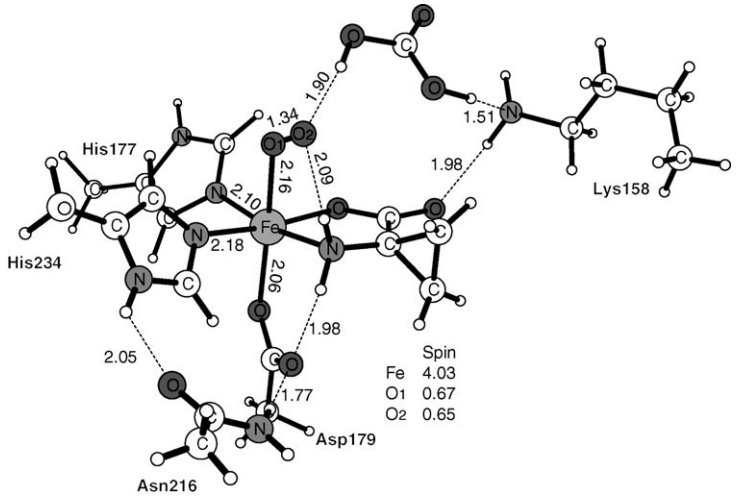

Figure 5. Optimized geometry of the dioxygen-bound iron(II) complex (S=3). Relevant distances and spin populations are shown.

Table 1. Relevant bond distances and computed spin distributions for dioxygen-bound non-heme iron(II) complexes in ACCO characterized by different total spins S. Relative energies (ΔE) are shown together with an estimate of the entropy correction ($-T\Delta S$) to the Gibbs free energy.

	Distance [Å]		Spin			[kcal mol^{-1}]	
	Fe–O	O1–O2	Fe	O1	O2	ΔE	$-T\Delta S$[a]
S=3	2.16	1.34	4.03	0.67	0.65	0	0
S=2	2.07	1.37	4.07	−0.19	−0.56	1.9	1.8
S=1	1.97	1.37	1.03	0.40	0.57	5.1	6.5

[a] Entropy corrections are obtained with a smaller model with no frozen coordinates (see Supporting Information).

characterized by low-spin coupling on ferric ion with its single unpaired electron ferromagnetically coupled with the unpaired electron of superoxide ion, and lies rather high in energy especially because of the significant entropy correction. This correction has been estimated from a smaller model without frozen coordinates (see Figure S1 in the Supporting Information). Thus, it is concluded likely that iron remains in the high-spin configuration also upon dioxygen binding. In the triplet state with high-spin iron, dioxygen is not bound and has thus not been considered. In the septet (S = 3) and the quintet (S = 2) states the electrons of the high-spin ferric ion are ferro- or antiferromagnetically coupled with the unpaired electron of superoxide anion.

The process of ethylene formation is likely to involve the formation of a substrate radical at the amino nitrogen of ACC as shown in the mechanism of Figure 2. No low-lying transition state structure could be located for the formation of such a radical starting from the dioxygen-bound iron(II) complex of Figure 5. The only way for the reaction to proceed is thus the reduction of this complex by ascorbate, as indeed shown in the mechanism of Figure 2. The present work does not address the energetics of electron transfer mainly because of the lack of experimental information on this process. For example, it is known that ascorbate is the overall source of the reducing equivalents (at least in vitro), but it is also known that in the absence of ascorbate, ethylene is still produced by ACCO in a single turnover and the reaction leads to a ferric complex. It is useful to recall that a similar one-electron reduction of the dioxygen-bound iron(II) complex by an external donor occurs in another non-heme iron(II) enzyme, namely, naphthalene dioxygenase.[42,43] For this enzyme, calculations suggest that the electron transfer step is an exothermic process that cancels the entropy loss and thus the endergonicity of the dioxygen binding process.[44] ACCO might adopt the same strategy as the one of naphthalene dioxygenase.

The iron(II)–superoxo moiety: The one-electron transfer to the ACC-Fe^{II}-O$_2$ complex leads to the iron(II)–superoxide depicted in Figure 6a, where relevant geometrical details and computed spin populations are reported for the S=$^5/_2$ spin state. This complex is found to be isoenergetic (ΔE = −0.03 kcal mol^{-1}) with the iron(III)–hydroperoxide generated upon one-electron transfer from iron to superoxide (Figure 6b). Oxidation of the metal ion is coupled with a transfer of a proton from carbonic acid. The superoxide/hydroperoxide transformation is found to require a negligible activation barrier. However, as seen below this proton transfer is not part of the reaction pathway in the mechanism presently suggested.

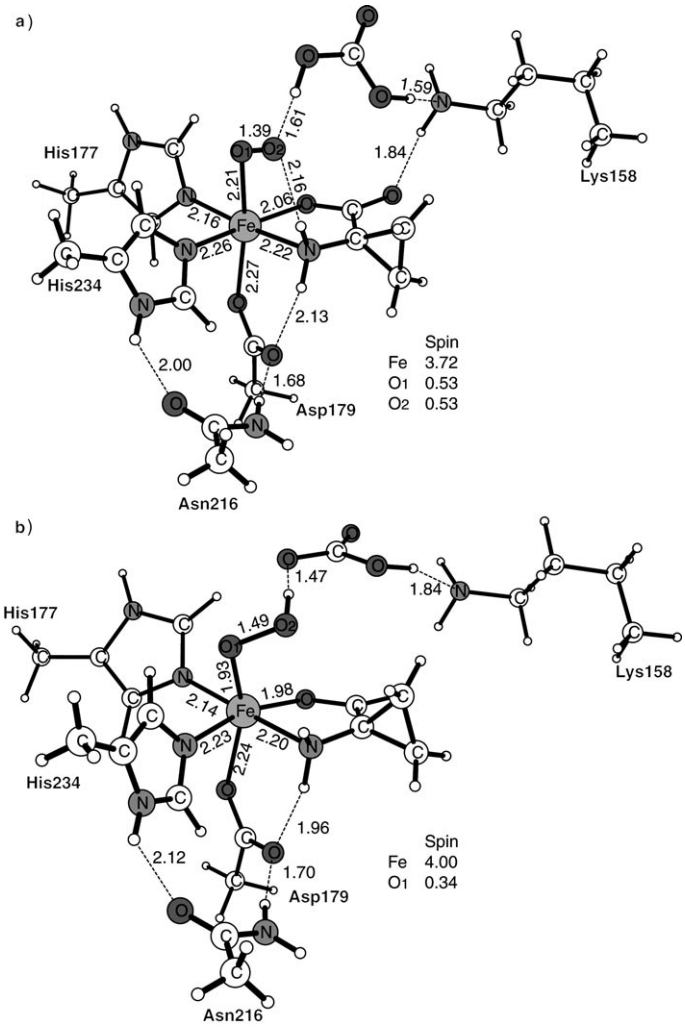

Figure 6. Optimized geometries of the iron(II)–superoxide and the iron(III)–hydroperoxide (S=5/2). Relevant distances and spin populations are shown.

Calculations show that the B3LYP functional gives a near-zero enthalpic spin splitting between the S = $^5/_2$ and $^1/_2$ states of the iron(III)–hydroperoxide of Figure 6b, with the low-spin state lying only 0.5 kcal mol^{-1} higher than the high-spin state. However, as highlighted above in Table 1, the entropy contribution might significantly affect the spin splitting between low- and high-spin states and thus a smaller model (see Figure S2, Supporting Information) without frozen coordinates was optimized to estimate $-T\Delta S$ for this ferric complex. On the free energy scale, the S=$^5/_2$ state then becomes more stable than the S=$^1/_2$ state by more than 5 kcal mol^{-1}. The S=$^1/_2$ state of the iron(II)–superoxide could not be optimized because it always decayed to the

iron(III)–hydroperoxide. The quartet spin state is also possible and, when optimized, leads to an iron(II)–superoxide where the unpaired electron located on the superoxide is antiparallel with respect to the four unpaired electrons of the ferrous ion. Within the accuracy of the calculations, this complex is found to be degenerate with the $S=^5/_2$ complex of Figure 6a. On the basis of all these results, the energy of the $S=^5/_2$ iron(II)–superoxide is taken as reference in the following discussion. Three potential energy surfaces, namely, the doublet, the quartet and the sextet surfaces, are then accessible for the reaction of ethylene formation, and two possible reactants (Fe^{II}-$O_2^{-\bullet}$ and Fe^{III}-OOH) can lead to the substrate radical and the high-valent iron–oxo species.

Formation of a radical intermediate: In the iron(II)–superoxo species, formation of a radical on ACC is found to be triggered by bound superoxide, which is capable of abstracting the hydrogen atom from the amino group of the substrate with a relatively low energy barrier. As shown in Figure 6a, the reactive amino group involved in the hydrogen atom abstraction process is bound to the metal. The corresponding transition state structure TS1 is shown in Figure 7a. This chemical transformation occurring on the sextet potential energy surface leads to an intermediate that can be formally described as an iron(II)–hydroperoxide with a bound radical (IN1 of Figure 7b). The computed spin populations of this intermediate (the iron spin population is 3.98 and the spin population of the amino nitrogen is 0.41) indicate that the oxidation state of iron is between Fe^{II} and Fe^{III} (see Computational Details).[31] Because of the corrections added to the final energy (solvent and zero-point effects as explained in the Computational Details), the transition state structures for the hydrogen atom abstraction (TS1) and the subsequent intermediate (IN1) are nearly degenerate as shown in the energy diagrams of Figure 8.

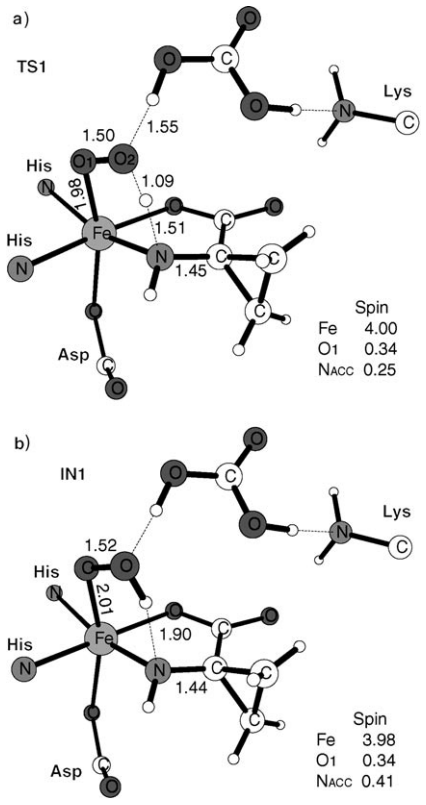

Figure 7. Optimized geometries of the transition state structure TS1 (a) and the subsequent intermediate IN1 (b) in the hydrogen atom abstraction step by bound superoxide. For clarity, only part of the model structure is shown. Relevant distances [Å] and spin populations are reported.

After a radical has been created on the ACC ligand, two different pathways are possible. In one case, the cyclopropane ring of the iron(II)–hydroperoxide IN1 undergoes C–C bond cleavage, which is followed by the heterolytic cleavage of the O–O bond in the hydroperoxo moiety (lower energy diagram of Figure 8). Alternatively the two steps may occur in a reverse order with the O–O bond cleavage preceding the C–C bond cleavage (upper energy diagram of Figure 8). As discussed in detail below, the present calculations suggest that the former is favored.

Cyclopropane ring opening before O–O bond cleavage (lower energy diagram in Figure 8) involves the transition state structure TS2cc of Figure 9a, where the computed spin populations are indicative of a developing propyl radical (a spin population of 0.66 is computed at the carbon atom in TS2cc). The C–C bond cleavage, which requires an energy barrier of 20.8 kcal mol^{-1}, transfers the radical character of the ACC substrate from nitrogen to carbon and yields the iron(II)–hydroperoxide IN2cc of Figure 9b. Subsequently, with an energy barrier at 19.2 kcal mol^{-1}, the O–O bond undergoes heterolysis through the transition state structure TS3oo of Figure 9c. In this step, the adjacent bicarbonate plays an essential role by delivering an extra proton to the distal oxygen atom; protonation of the distal oxygen allows a low-barrier O–O bond cleavage by means of the formation of a good leaving group namely, water; without protonation the O–O bond heterolysis is prevented. O–O bond cleavage and water release results in the formation of the iron(IV)–oxo species IN3 of Figure 10; the computed spin populations of 3.00 on iron and 0.63 on the oxo group and the short Fe–O distance (1.66 Å) are consistent with previous studies of high-spin Fe^{IV}=O complexes.[31,45,46–49]

The alternative pathway (upper energy diagram of Figure 8), where heterolysis of the O–O bond occurs before the C–C bond cleavage, passes through a transition state structure (TS2oo of Figure 11a) that lies 23.8 kcal mol^{-1} higher in energy than the iron(II)–superoxide reactant. The product of the cleavage, which is coupled with a proton transfer from the adjacent bicarbonate, has an energy of +6.5 kcal mol^{-1} and leads to an iron(IV)–oxo intermediate (IN2oo) with a radical localized on the amino group of bound ACC as shown in Figure 11b. The iron-oxo moiety is again characterized by a short Fe–O distance and by the typical spin population of 3 on iron and 0.6–0.7 on the oxo group. The radical can then be transferred from nitrogen to the carbon atom of the propyl group of ACC through C–C bond cleavage that involves the transition state structure TS3cc shown in Figure 11c. This step requires a barrier of

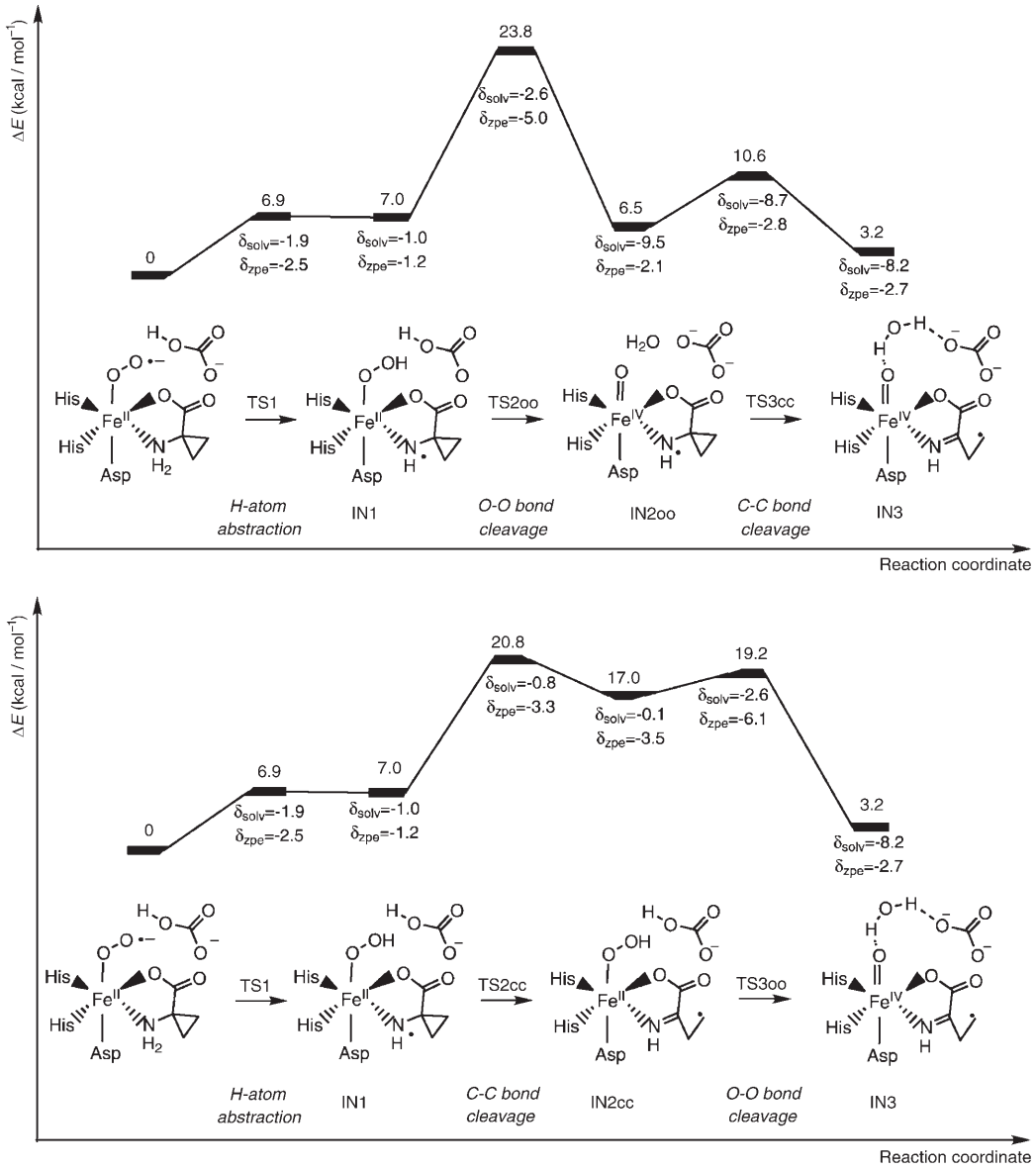

Figure 8. Energy diagrams [kcal mol^{-1}] for two possible pathways leading to the iron(IV)–oxo intermediate and a radical substrate in ACCO catalysis. In the lower diagram, the C–C bond cleavage of the cyclopropane ring precedes the O–O bond cleavage. The two steps occur in a reversed way for the upper diagram. Corrections to the final energy due to solvent and zero-point effects (δ_{solv} and δ_{zpe}, respectively) are also reported in kcal mol^{-1}.

4.1 kcal mol^{-1} and yields the other iron(IV)–oxo intermediate IN3 (Figure 10). It can be noted here that zero-point effects help to lower the energy barriers in the cleavage steps and that release of a water molecule directly after O–O bond heterolysis is likely to be the origin of the unusually large solvent effects, which lower the energetics by 8–9 kcal mol^{-1}, as reported in Figure 8.

O–O Bond cleavage occurring before cyclopropane ring opening has a barrier of 23.8 kcal mol^{-1} compared with the 19.2 kcal mol^{-1} required if the O–O bond is cleaved after ring opening. The difference can be explained in terms of the actual oxidation state of the metal during the O–O bond cleavage. As discussed above, before ring opening, the O–O bond cleavage occurs in a complex that can be described in terms of two resonance structures: an iron(II)–hydroperoxide with a bound nitrogen radical and an iron(III)–hydroperoxide with no radical on the ligand. However, after ring opening, the metal is clearly in the ferrous oxidation state, and the radical is fully transferred to the carbon which hosts a spin population of 1. The lower oxidation state of the metal (i.e., iron in the ferrous state) is likely to decrease the barrier for the O–O bond heterolysis.

Since the pathway starting with ring opening involves a lower barrier (20.8 kcal mol^{-1} associated with C–C bond cleavage) than the one for the other chemical route starting with O–O bond heterolysis (23.8 kcal mol^{-1} associated with O–O bond cleavage), the present investigation favors the formation of the iron(IV)–oxo species through opening of

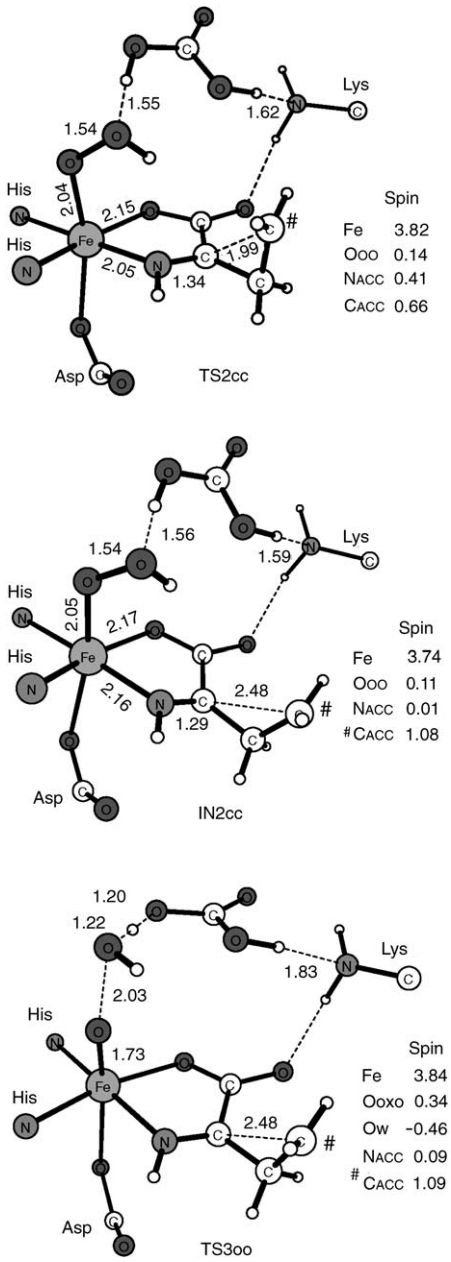

Figure 9. Optimized geometries of the transition state TS2cc in the C–C bond cleavage (top), of the following iron(II)–peroxide intermediate IN2cc (middle), and of the transition state TS3oo in the subsequent O–O bond heterolysis (bottom). For clarity, only part of the model structure is shown. Relevant distances [Å] and spin populations are reported.

the cyclopropane ring followed by O–O bond heterolysis. However, it should be noted that the accuracy of the present computational approach (3–5 kcal mol^{-1} as discussed in the computational details) does not allow us to discard the other route completely.

Since the S = $^1/_2$ state of the iron(II)–superoxide always decays to the corresponding iron(III)–hydroperoxide by means of a proton transfer from the adjacent bicarbonate, the hydrogen atom abstraction step by bound superoxide could not be investigated along the doublet potential energy

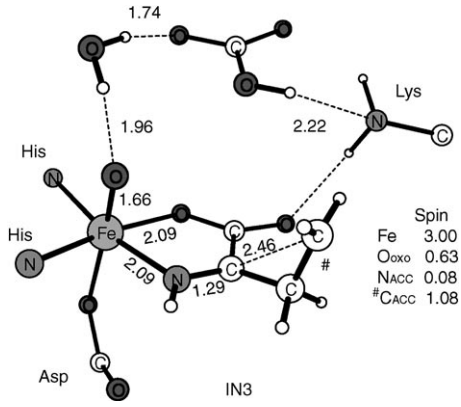

Figure 10. Optimized geometry of the iron(IV)–oxo intermediate IN3 following the cleavage of the O–O and C–C bonds in the iron(II)–peroxide moiety with the bound substrate radical. For clarity, only part of the model structure is shown. Relevant distances [Å] and spin populations are reported.

surface. In light of the result that the S = $^3/_2$ and $^5/_2$ states of the iron(II)–superoxide were computed to be nearly degenerate, the quartet potential energy surface was not probed in detail because it is expected to behave as the sextet one.

Besides the two routes for the O–O bond heterolysis discussed above and depicted in the energy diagrams of Figure 8, another pathway leading to the O–O bond cleavage needs to be considered. Calculations show that the ferric-hydroperoxide of Figure 6b might undergo O–O bond homolysis with a relatively low activation barrier. This chemical transformation, which implicates release of a hydroxyl radical, is found to occur along the doublet potential energy surface and requires an activation energy of ΔE = 25.6 kcal mol^{-1} (see Figure S3, Supporting information). It should be noted that this barrier is about 5 kcal mol^{-1} higher than the one computed for the heterolysis on the sextet potential energy surface (ΔE = 20.8 kcal mol^{-1}). On the free energy scale, it is expected that the thermal correction to the Gibbs free energy increases the difference by at least 2–3 kcal mol^{-1} since this transformation occurs on the S = $^1/_2$ potential energy surface while the ground state is instead characterized by a high-spin configuration on the metal. As discussed above (see for example Table 1) the entropy correction stabilizes the high-spin state over the low-spin state by a few kcal mol^{-1}. It is therefore concluded that the homolytic pathway is significantly disfavored over the heterolytic one.

It will be shown below that the iron(IV)–oxo species IN3 of Figure 10 can lead to ethylene release without any significant energy barrier. From the energy diagram reported in Figure 8 it is then possible to conclude that the slow step in ethylene formation is either the O–O bond or the C–C bond cleavage, both of which occur with rather similar activation barriers. If the first two steps of the ACCO catalytic cycle, namely substrate binding and electron transfer (Figure 2) generating ACC-Fe^{II}-$O_2^{-\bullet}$, result in an exergonic process (or even slightly endergonic by 1–2 kcal mol^{-1}), the

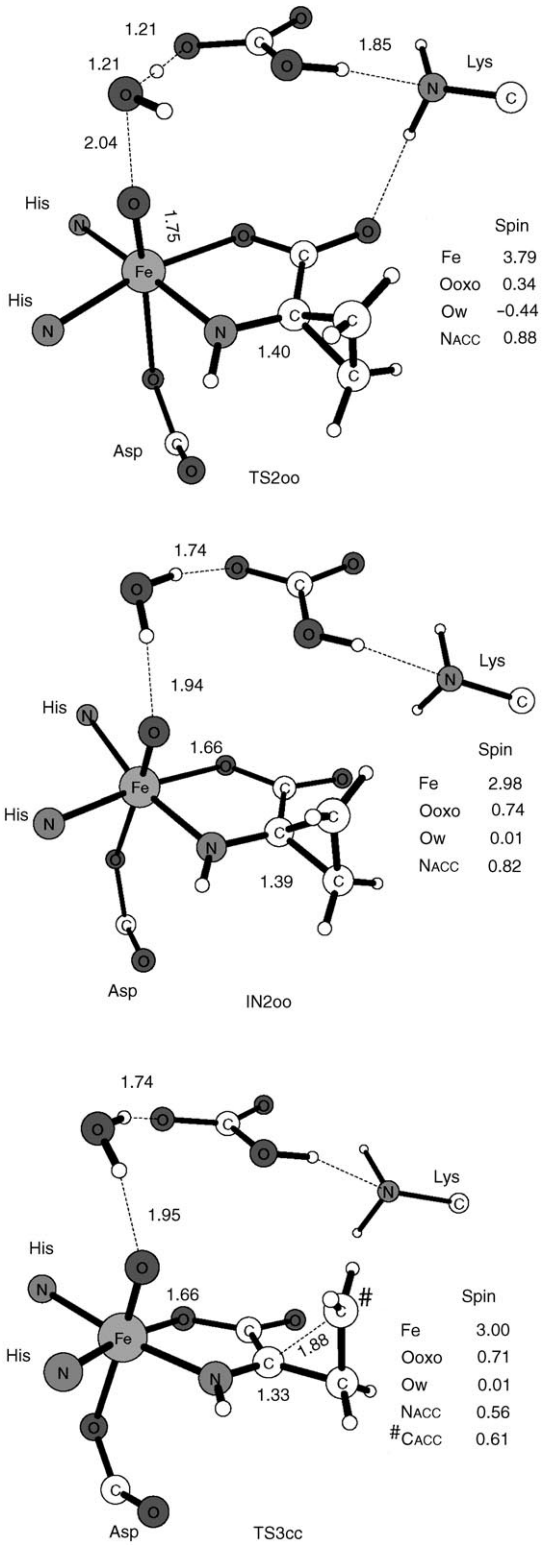

Figure 11. Optimized geometries of the transition state TS2oo in the O–O bond heterolysis (top), of the following iron(IV)–oxo intermediate IN2oo (middle), and of the transition state TS3cc in the subsequent C–C bond cleavage (bottom). For clarity, only part of the model structure is shown. Relevant distances [Å] and spin populations are reported.

computed energy barrier of 20.8 kcal mol^{-1} for the formation of the high-valent iron–oxo species is in excellent agreement with the one obtained by means of transition state theory from experimental kinetic data (18–19 kcal mol^{-1}).[15] No other pathways with lower barriers could be identified. Alternative mechanisms where, for example, bicarbonate binds in the first coordination sphere, or where ascorbate plays a more active role, or where CO_2 is the actual activator could be envisioned. An interesting possibility that was explored was whether a peroxocarbonate obtained from the reaction of bound superoxide and CO_2 could undergo C–C and O–O bond cleavage with lower activation energies. Indeed experimental studies on biomimetic systems clearly point at the feasibility of a reversible O–O bond cleavage in iron–peroxocarbonate complexes.[50] However, the present computational modeling indicates that this pathway does not involve lower activation barriers in the ethylene forming enzyme (see Figures S4 and S5, Supporting Information).

Catalytic role of bicarbonate: In order to test the catalytic role of bicarbonate, the steps leading to the formation of a radical intermediate were investigated with a model lacking the HCO_3^- group. These investigations were limited only to the steps depicted in the lower part of Figure 8, since these transformations involve the lowest energy rate-limiting (chemical) step of the catalytic reaction. The energy (without the ZPE) obtained for this model is shortly discussed here, while the critical structures are presented in the Supporting Information.

The structure of the reactant iron(II)–superoxide complex is very similar to that obtained for a model including bicarbonate anion (compare Figure 6 and S9). Like before, the charge separation is destroyed, but now the carboxylic group of the substrate (ACC) abstracts the proton form the protonated form of lysine 158.

Hydrogen atom transfer from the NH_2 group of ACC to the superoxide anion involves a barrier of 10.6 kcal mol^{-1} and leads to an intermediate IN1 which lies at 10.4 kcal mol^{-1}. These energies obtained for a model with bicarbonate anion (without ZPE) are 9.4 and 8.2 kcal mol^{-1}, respectively. Similarly, the subsequent C–C bond cleavage involves a barrier very similar to that obtained for the model with bicarbonate, that is, 26.1 and 24.1 kcal mol^{-1} for the model without and with bicarbonate, respectively (for the structure see Figure S10, Supporting Information). Thus, up to the intermediate IN2cc, which was computed to lie at 19.4 and 20.5 kcal mol^{-1} for the models with and without bicarbonate, the presence of bicarbonate has a modest (up to 2 kcal mol^{-1}) impact on the energetics. However, the O–O cleavage step, which involves a protonation of the leaving OH group, is significantly affected, since the barrier calculated for a model without bicarbonate is 38.2 kcal mol^{-1}, while in the presence of this group the barrier (without ZPE) is 25.3 kcal mol^{-1}. This 12.9 kcal mol^{-1} catalytic effect of the HCO_3^- group is best understood if one compares the structures of the two transition states (Figure 9 and S11). In the case of the model with bicarbonate (Figure 9) the proton de-

livered to the leaving OH group comes from the H_2CO_3 moiety already hydrogen bonding to the OOH group in the preceding intermediate (IN2cc). In the model without bicarbonate (Figure S11) a strong hydrogen bond between the protonated carboxylic group of the substrate and Lys158 and the coordination bond between the same carboxylic group and iron have to be broken in order to deliver the proton to the leaving OH group in the TS structure. Thus, it is concluded that the most likely role of bicarbonate in the catalytic reaction of ACCO is to facilitate a proton transfer from Lys158 to the leaving OH group during the O–O bond cleavage.

Release of ethylene: Calculations show that the iron(IV)–oxo intermediate with the bound substrate radical (IN3 of Figure 10) generates ethylene and cyanoformate with very low energy barriers. As summarized in Figure 12, the second

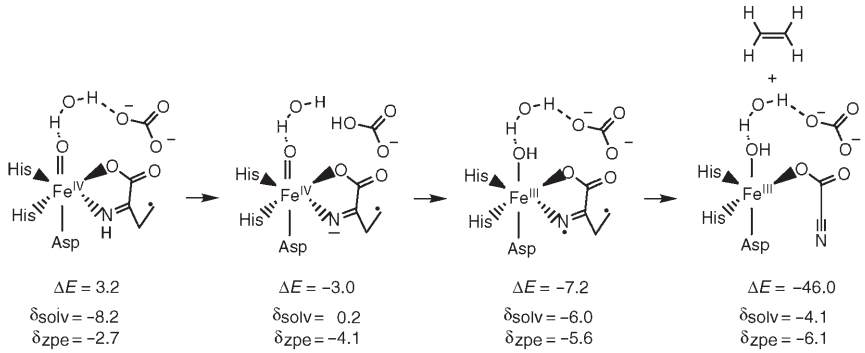

Figure 12. Decomposition of the iron(IV)–oxo intermediate IN3 producing ethylene and cyanoformate. Relative energies [kcal mol^{-1}] with respect to the iron(II)–superoxide reactant are reported.

C–C bond cleavage producing ethylene is preceded by deprotonation of the imine group of the ACC radical and protonation of the oxo group. This sequential proton transfer is mediated by water and bicarbonate: first the adjacent bicarbonate becomes protonated through the assistance of the water molecule; then the proton is transferred to the oxo group again through water. No low-lying transition state structure for the second C–C bond cleavage could be optimized before this deprotonation step. Deprotonation of the imine group leads to an intermediate that can be described either as an iron(IV) complex or as an iron(III) species with a biradical ligand.

While deprotonation of the imine group requires a nonzero energy barrier (about 3 kcal mol^{-1}) with respect to the preceding intermediate, the other two steps occur with negligible activation energies (see Figures S6–S8, Supporting Information). The overall reaction is exergonic by 46.0 kcal mol^{-1} and leads to a ferric complex which can then be reduced to the initial ferrous oxidation state upon transfer of a second external electron, possibly from ascorbate or the semidehydroascorbate radical. The exact pathway of decomposition of cyanoformate to CO_2 and CN^- has not been addressed in the present study but it is known that cyanoformic acid is unstable with respect to its constituents, CN^- and CO_2.[17] Thus, it is assumed that this reaction occurs easily in solution.

Conclusions

The present theoretical study addresses the details of the reaction pathway in the ethylene forming enzyme (ACCO) after the substrates ACC and O_2 bind to the mononuclear iron(II) complex located in the active site and after an external electron reduces this complex. The study has been performed with a model system including a bicarbonate anion in the second coordination sphere (Figure 6). In this way the role of bicarbonate could be explored.

As shown in the proposed mechanism depicted in Figure 2, the catalytic cycle of this enzyme is likely to pass through the formation of a radical on ACC. Calculations first show that the ACC-Fe^{II}-O_2 complex alone is not capable of generating any radical on the ACC substrate. The only plausible alternative step is then the one-electron reduction of the metal complex generating an iron(II)–superoxo species, which is considered to be the actual reactive oxidizing species in the current investigation. Bound superoxide is able to perform a hydrogen atom abstraction from the amino group of the substrate with a relatively low activation barrier as shown in the energy diagram of Figure 8. This step leads to an intermediate that can be formally described as an iron(II)–hydroperoxide with a bound radical located on the amino nitrogen of ACC. Since the computed spin population on nitrogen is only 0.4 as shown in Figure 7, this species may be regarded to be in resonance with another structure, namely an iron(III)–hydroperoxide with no radical on ACC. Although, the role of bicarbonate in this step is one of a mere spectator, it should be noted that the iron(II)–superoxo species is computed isoenergetic with the iron(III)–hydroperoxo species obtained upon proton transfer from bicarbonate and an electron transfer from the ferrous ion. This species in the low-spin state might undergo O–O bond homolysis with a rather high activation barrier and thus it can be considered unreactive. Because the hydrogen atom abstraction step by bound superoxide is found to be an essential step in the catalytic cycle, it is possible that bicarbonate plays an important role by properly adjusting the microenvironment of the active site to prevent protonation of superoxide by external agents. This proposal may explain why, at least some forms of ACCO, are inefficient catalysts in vitro and prone to oxidative damage.

After creation of a radical on the ACC nitrogen, the iron(II)–hydroperoxide can follow two different fates: either it undergoes O–O bond heterolysis giving a high-valent iron–oxo species and a radical on the ACC nitrogen (upper energy diagram of Figure 8), or the radical can be transferred from nitrogen to a carbon atom through ring opening of the cyclopropane ring (lower energy diagram of Figure 8). The present computations indicate that the latter pathway (i.e., first ring opening and then O–O bond cleavage) is favored over the former and it requires an energy barrier which is about 3 kcal mol^{-1} lower.

In this part of the catalytic cycle, bicarbonate plays the role of proton donor, providing the extra proton needed to cleave the O–O bond. The heterolysis results in water release, where the two protons originate from ACC and bicarbonate. C–C bond cleavage and subsequent O–O bond heterolysis generate the key intermediate in the reaction catalyzed by ACCO: the Fe^{IV}=O species with a propyl radical. This species is characterized by a short Fe–O distance typical of iron(IV)–oxo species as discussed in previous theoretical works as well as in experimental investigations.[31,46,47] Calculations demonstrate that this species decomposes to ethylene and cyanoformate with very low activation barriers. These final steps first require deprotonation of the imine group as summarized in the reaction scheme reported in Figure 12.

The energies of intermediates and transition states lead to the conclusion that, once an external electron has been provided to the iron(II)–dioxygen complex, ethylene formation occurs via a very reactive radical species (the iron(IV)–oxo intermediate IN3 of Figure 10) with an energy barrier of about 20 kcal mol^{-1} (20.6 kcal mol^{-1} is the barrier for the C–C bond cleavage and 19.2 is that for the O–O bond cleavage). This activation barrier is in good agreement with that derived from experimental kinetic data on the basis of transition state theory.[15] It should be noted that this comparison is valid as long as binding of the two substrates O_2 and ACC to iron(II) and the one-electron transfer result in an exergonic process, or even a slightly endergonic one by a couple of kcal mol^{-1}. If this is the case, the energy of the iron(II)–superoxide can be taken as reference and the final barrier is thus approximately 20 kcal mol^{-1}. Notably, in naphthalene dioxygenase, a mononuclear non-heme iron enzyme belonging to the same super-family as ACCO, the free energy change for binding of dioxygen and the one-electron transfer from an external donor is near zero. It is therefore reasonable to assume that formation of the iron(II)–superoxide is not an endergonic process which requires very high activation barriers in the ethylene-forming enzyme.

[1] H. Kende, J. A. D. Zeevaart, *Plant Cell* **1997**, *9*, 1197–1210.
[2] H. Kende, *Annu. Rev. Plant Physiol. Plant Mol. Biol.* **1993**, *44*, 283–307.
[3] J. R. Ecker, *Science* **1995**, *268*, 667–675.
[4] S. F. Yang, N. E. Hoffman, *Annu. Rev. Plant Physiol. Plant Mol. Biol.* **1984**, *35*, 155–189.
[5] Z. Zhang, J.-s. Ren, I. J. Clifton, C. J. Schofield, *Chem. Biol.* **2004**, *11*, 1383–1394.
[6] M. Costas, M. P. Mehn, M. P. Jensen, L. Que Jr., *Chem. Rev.* **2004**, *104*, 939–986.
[7] E. I. Solomon, T. C. Brunold, M. I. Davis, J. N. Kemseley, S.-K. Lee, N. Lehnert, F. Neese, A. J. Skulan, Y.-S. Yang, J. Zhou, *Chem. Rev.* **2000**, *100*, 235–349.
[8] K. Koehntop, J. P. Emerson, L. Que Jr., *J. Biol. Inorg. Chem.* **2005**, *10*, 87–93.
[9] L. Que Jr., *Nat. Struct. Biol.* **2000**, *7*, 182–184.
[10] E. L. Hegg, L. Que Jr., *Eur. J. Biochem.* **1997**, *250*, 625–629.
[11] A. Bassan, T. Borowski, P. E. M. Siegbahn, *Dalton Trans.* **2004**, *20*, 3153–3162.
[12] G. Peiser, T.-T. Wang, N. E. Hoffman, S. F. Yang, H. W. Liu, C. Walsh, *Proc. Natl. Acad. Sci. USA* **1984**, *81*, 3059–3063.
[13] J. G. Dong, J. C. Fernandez-Maculet, S. F. Yang, *Proc. Natl. Acad. Sci. USA* **1992**, *89*, 9789–9793.
[14] P. John, *Physiol. Plant.* **1997**, *100*, 583–592.
[15] J. S. Thrower, R. I. Blalock, J. P. Klinman, *Biochemistry* **2001**, *40*, 9717–9724.
[16] A. M. Rockiln, K. Kato, H.-w. Liu, L. Que Jr., J. D. Lipscomb, *J. Biol. Inorg. Chem.* **2004**, *9*, 171–182.
[17] M. C. Pirrung, *Acc. Chem. Res.* **1999**, *32*, 711–718.
[18] A. M. Rocklin, D. L. Tierney, V. Kofman, N. M. W. Brunhuber, B. Hoffman, R. E. Christoffersen, N. O.. Reich, J. D. Lipscomb, *Proc. Natl. Acad. Sci. USA* **1999**, *96*, 7905–7909.
[19] D. L. Tierney, A. M. Rocklin, J. D. Lipscomb, L. Que Jr., B. M. Hoffman, *J. Am. Chem. Soc.* **2005**, *127*, 7005–7013.
[20] D. G. McRae, J. E. Baker, J. E. Thompson, *Plant Cell Physiol.* **1982**, *23*, 375–383.
[21] J. N. Barlow, Z. Zhang, P. John, J. E. Baldwin, C. J. Schofield, *Biochemistry* **1997**, *36*, 3563–3569.
[22] J. Zhou, A. M. Rocklin, J. D. Lipscomb, L. Que Jr., E. I. Solomon, *J. Am. Chem. Soc.* **2002**, *124*, 4602–4609.
[23] A. D. Becke, *J. Chem. Phys.* **1993**, *98*, 5648–5652.
[24] P. J. Stevens, F. J. Devlin, C. F. Chablowski, M. J. Frisch, *J. Phys. Chem.* **1994**, *98*, 11623–11627.
[25] C. Lee, W. Yang, R. G. Parr, *Phys. Rev. B* **1988**, *37*, 785–789.
[26] Jaguar 4.0. Schrödinger, Inc., Portland, Oregon, **2000**.
[27] Gaussian98, M. J. Frisch, G. W. Trucks, H. B. Schlegel, G. E. Scuseria, M. A. Robb, J. R. Cheeseman, V. G. Zakrzewski, Montgomery J. A. Jr., R. E. Stratmann, J. C. Burant, S. Dapprich, J. M. Millan, A. D. Daniels, K. N. Kudin, M. C. Strain, O. Farkas, J. Tomasi, V. Barone, M. Cossi, R. Cammi, B. Mennucci, C. Pomelli, C. Adamo, S. Clifford, J. Ochterski, G. A. Petersson, P. Y. Ayala, Q. Cui, K. Morokuma, D. K. Malick, A. D. Rabuck, K. Raghavachari, J. B. Foresman, J. Cioslowski, J. V. Ortiz, B. B. Stefanov, G. Liu, A. Liashenko, P. Piskorz, I. Komaromi, R. Gomperts, R. L. Martin, D. J. Fox, T. Keith, Al-M. A. Laham, C. Y. Peng, A. Nanayakkara, C. Gonzalez, M. Challacombe, P. M. W. Gill, B. Johnson, W. Chen, M. W. Wong, J. L. Andres, M. Head-Gordon, E. S. Replogle, J. A. Pople, Gaussian Inc., Pittsburgh, PA, **1998**.
[28] P. J. Hay, W. R. Wadt, *J. Chem. Phys.* **1985**, *82*, 299–310.
[29] D. J. Tannor, B. Marten, R. Murphy, R. A. Friesner, D. Sitkoff, A. Nicholls, B. Honig, M. Ringnalda, W. A. Goddard III, *J. Am. Chem. Soc.* **1994**, *116*, 11875–11882.
[30] B. Marten, K. Kim, C. Cortis, R. A. Friesner, R. B. Murphy, M. Ringnalda, D. Sitkoff, B. Honig, *J. Phys. Chem.* **1996**, *100*, 11775–11788.
[31] A. Bassan, PhD thesis, Stockholm University, Stockholm, Sweden, **2004**.
[32] L. A. Curtiss, K. Raghavachari, P. C. Redfern, J. A. Pople, *J. Chem. Phys.* **2000**, *112*, 7374–7383.
[33] L. A. Curtiss, K. Raghavachari, P. C. Redfern, J. A. Pople, *J. Chem. Phys.* **1997**, *106*, 1063–1079.
[34] P. E. M. Siegbahn, M. R. A. Blomberg, *Chem. Rev.* **2000**, *100*, 421–437.
[35] M. R. A. Blomberg, P. E. M. Siegbahn, *J. Phys. Chem. B* **2001**, *105*, 9375–9386.

[36] P. E. M. Siegbahn, M. R. A. Blomberg, *Annu. Rev. Phys. Chem.* **1999**, *50*, 221–249.
[37] M. R. A. Blomberg, P. E. M. Siegbahn, In *Transition State Modeling for Catalysis* (Eds.: D. G. Truhlar, K. Morokuma), American Chemical Society, Washington DC, **1999**.
[38] J. V. Lay, A. G. Prescott, P. G. Thomas, P. John, *Eur. J. Biochem.* **1996**, *242*, 228–234.
[39] A. Bassan, M. R. A. Blomberg, P. E. M. Siegbahn, *Chem. Eur. J.* **2003**, *9*, 106–115.
[40] T. Borowski, A. Bassan, P. E. M. Siegbahn, *Chem. Eur. J.* **2004**, *10*, 1031–1041.
[41] A. Bassan, M. R. A. Blomberg, P. E. M. Siegbahn, *J. Biol. Inorg. Chem.* **2004**, *9*, 439–452.
[42] D. T. Gibson, R. E. Parales, *Curr. Opin. Biotechnol.* **2000**, *11*, 235–243.
[43] B. Kauppi, K. Lee, E. Carredano, R. E. Parales, D. T. Gibson, H. Eklund, S. Ramaswamy, *Structure* **1998**, *6*, 571–586.
[44] A. Bassan, M. R. A. Blomberg, T. Borowski, P. E. M. Siegbahn, *J. Phys. Chem. B* **2004**, *108*, 13031–13041.
[45] A. Bassan, M. R. A. Blomberg, P. E. M. Siegbahn, *Chem. Eur. J.* **2003**, *9*, 4055–4067.
[46] E. J. Klinker, J. Kaizer, W. W. Brennessel, N. L. Woodrum, C. J. Cramer, L. Que Jr., *Angew. Chem.* **2005**, *117*, 3756–3760; *Angew. Chem. Int. Ed.* **2005**, *44*, 3690–3694.
[47] E. J. Klinker, J. Kaizer, W. W. Brennessel, W. N. L. , C. J. Cramer, L. Que Jr., *Angew. Chem.* **2005**, *117*, 3756–3760.
[48] J. C. Price, E. W. Barr, B. Tirupati, J. M. Bollinger, C. Krebs, *Biochemistry* **2003**, *42*, 7497–7508.
[49] D. A. Proshlyakov, T. F. Henshaw, G. R. Monterosso, M. J. Ryle, R. P. Hausinger, *J. Am. Chem. Soc.* **2004**, *126*, 1022–1023.
[50] H. Furutachi, K. Hashimoto, S. Nagamoto, T. Endo, S. Fijinami, Y. Watanabe, T. Kitagawa, M. Sukuzi, *J. Am. Chem. Soc.* **2005**, *127*, 4550–4551.

Received: November 24, 2005
Revised: April 18, 2006
Published online: August 25, 2006

